Solvent-Dispersed Benzothiadiazole-Tetrathiafulvalene Single-Crystal Nanowires and Their Application in Field-Effect Transistors

ARTICLE *in* ACS APPLIED MATERIALS & INTERFACES · MARCH 2013

Impact Factor: 6.72 · DOI: 10.1021/am3025036 · Source: PubMed

8 AUTHORS, INCLUDING:

Hin-Lap Yip
South China University of Technology
123 PUBLICATIONS **6,894** CITATIONS
SEE PROFILE

Alex K-Y Jen
University of Washington Seattle
391 PUBLICATIONS **15,968** CITATIONS
SEE PROFILE

ACS APPLIED MATERIALS & INTERFACES

Forum Article

www.acsami.org

Solvent-Dispersed Benzothiadiazole-Tetrathiafulvalene Single-Crystal Nanowires and Their Application in Field-Effect Transistors

Neil M. Tucker,[†] Alejandro L. Briseno,[†] Orb Acton,[‡] Hin-Lap Yip,[‡] Hong Ma,[‡] Samson A. Jenekhe,*[,†,§] Younan Xia,[†] and Alex K.-Y. Jen*[,†,‡]

[†]Department of Chemistry, [‡]Department of Materials Science and Engineering, and [§]Department of Chemical Engineering, University of Washington, Seattle, Washington 98195, United States

Supporting Information

ABSTRACT: A new organic semiconductor (BT-TTF) based on molecular moieties of benzothiadiazole and tetrathiafulvalene was designed and synthesized, and its structure, molecular packing and charge-transporting properties were determined. Thermal properties, electrochemical behaviors, and optical absorption of this molecule were studied by using differential scanning calorimetry/thermal gravimetric analysis, cyclic voltammetry, and ultraviolet−visible spectroscopy, respectively. Its bulk and nanowire single crystals were prepared and characterized by X-ray crystallography, scanning electron microscopy, transmission electron microscopy, and field-effect transistors. It is found that short intermolecular S···S (3.41 Å), S···C (3.49 Å), and S···N (3.05 Å) contacts define the solid-state structure of BT-TTF single crystals which π-stack along the [100] with interplanar distances of 3.49 Å. Solvent-cast single-crystal nanowire transistors showed mobilities as large as 0.36 $cm^2/(V\ s)$ with current on/off ratios of 1×10^6. This study further illustrates the impact of molecular design and a demonstration of high-performance single-crystal nanowire transistors from the resulting semiconductor.

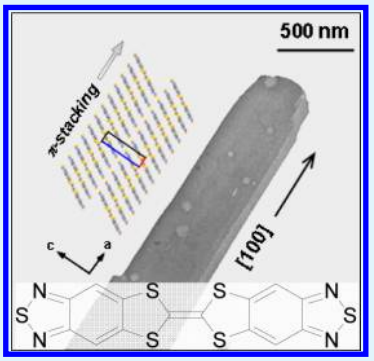

KEYWORDS: *organic semiconductor, single crystal, nanowire, field-effect transistor*

1. INTRODUCTION

The development of organic molecules as active components of electronic and optoelectronic devices has seen unprecedented progress in the past decade.[1−3] This attention is primarily due to the potential impact on large-area and low-cost fabrication of devices, integrated circuits, flexible displays, and in particular, organic field-effect transistors (OFETs).[4−6] One frequently used method of characterizing organic semiconductors is through a single-crystal OFET.[7] High charge-carrier mobilities have been demonstrated in single-crystal devices[7] as the organic crystal is free of grain boundaries and possesses a high degree of molecular order. However, single-crystal transistors are difficult to fabricate and device throughput is low.[7a,8]

Solution deposition of one-dimensional (1D) organic single-crystals has emerged as a promising approach to realizing high-performance transistors, integrated circuits, structure−property studies, and for facile device fabrication.[9,10] Organic semiconductors that pack face-to-face in the solid state are of particular interest for this technique since they are known to self-assemble into 1D nanostructures due to strong $\pi-\pi$ interactions.[9,10] This packing mode has also been correlated with high performance in OFETs.[11a,b]A review concerning the performance status of organic nanowire devices has been recently published to summarize assembly, properties, and applications of one-dimensional nanostructures of π-conjugated molecular systems.[11c]

Engineering linear/planar molecules to pack face-to-face is challenging because the interacting forces between organic molecules are relatively weak.[1] To induce face-to-face packing, we sought to introduce a variety of noncovalent interactions. Inspired by S···S interactions found in tetrathiafulvalene (TTF)[12] and electrostatic interactions found in 1,2,5-thiadiazole derivatives,[13] we created a hybrid of these two molecules in benzothiadiazole-tetrathiafulvalene (BT-TTF) (Scheme 1). In addition to increasing $\pi-\pi$ interactions, the electron deficient 1,2,5-thiadiazole moieties on either end of the TTF core are expected to enhance the air stability by decreasing the overall electron-donating property of the molecule.[14]

2. EXPERIMENTAL SECTION

2.1. Molecular Synthesis. All chemicals were purchased from Aldrich and used as received unless otherwise specified. Reactions were performed under an atmosphere of dry nitrogen. 2,1,3-Benzothiadiazole-5,6-bis(thiocyanate) was prepared according to the literature procedure.[15a] Melting points are uncorrected. Infrared spectra (KBr disc) were collected using a Perkin-Elmer 1720 FTIR spectrometer. ^1H and ^{13}C NMR spectra were recorded on a Bruker AV-500 FT NMR (500 MHz) spectrometer. High resolution electrospray ionization (ESI) mass spectra was obtained on a Bruker

Special Issue: Forum on Advancing Technology with Organic and Polymer Transistors

Received: October 29, 2012
Accepted: March 5, 2013

   dx.doi.org/10.1021/am3025036 | *ACS Appl. Mater. Interfaces* XXXX, XXX, XXX−XXX

Scheme 1. Synthesis of BT-TTF[a]

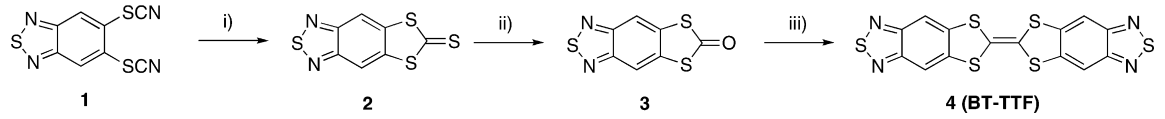

[a](i) Na_2S, H_2O, CS_2; (ii) $Hg(OAc)_2$, $CHCl_3$; (iii) $P(OEt)_3$, 120°C, 2 h.

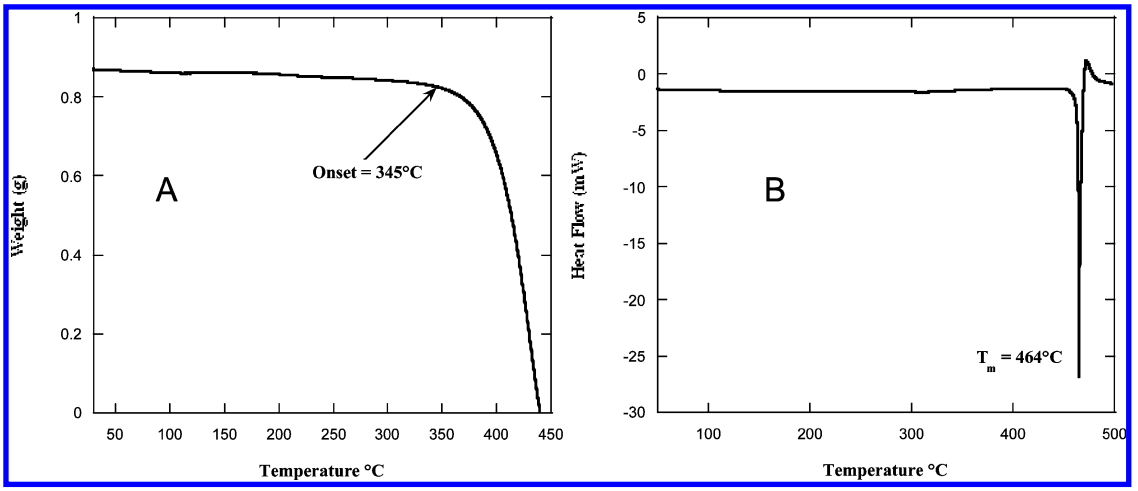

Figure 1. (A) TGA and (B) DSC of BT-TTF.

APEX Qe 47e: Fourier transform (Ion Cyclotron Resonance) mass spectrometer [FT(ICR)]MS by the UW Mass Spectrometry Center. High-resolution electron impact ionization (EI) mass spectra were obtained on a JEOL HX-110 by the UW Chemistry Mass Spectrometry Lab. Elemental analysis was determined at QTI (Whitehouse, NJ).

*[1,2,5]Thiadiazolo[3,4-f][1,3]benzodithiole-2-thione (**2**).* 2,1,3-Benzothiadiazole-5,6-bis(thiocyanate) **1** (0.55 g, 2.22 mmol) was added to a solution of sodium sulfide nonahydrate (1.8 g, 7.32 mmol) in degassed water (20 mL). The solution was heated to 70 °C for 30 min to produce a clear orange solution. The solution was cooled to 50 °C and carbon disulfide (2 mL) was added. The reaction stirred for 2 h during which time a solid precipitated from the solution. Upon cooling, the solid was filtered, washed with water, and air-dried to give of 3 (0.40 g, 75%) as a yellow solid. Mp 201−203 °C (from EtOH); ν_{max}(KBr disk)/cm^{-1} 1483 (m), 1438 (w), 2345 (w), 1240 (m), 1059 (s), 1018 (s) 889 (w), 860 (s), 840 (m), 818 (m), 700 (w), 649 (w), 530 (w), 510 (m), 448 (w), 423 (w), 409 (w); ^{1}H NMR (500 MHz; $CDCl_3$) δ (ppm): 8.12 (2 H, s); ^{13}C NMR (125 MHz; $CDCl_3$) δ (ppm): 211.6, 153.0, 144.3, 112.7; *m*/*z* (ESI) 242.9178 (m + H. $C_7H_2N_2S_4$ requires 241.9101).

*[1,2,5]Thiadiazolo[3,4-f][1,3]benzodithiole-2-one (**3**).* **2** (0.34g, 1.40 mmol) and mercury acetate (2eq, 0.89g, 2.80 mmol) were stirred for 2 h at room temperature in chloroform (15 mL) and acetic acid (7.0 mL). The reaction was then filtered through Celite and washed with a saturated sodium bicarbonate solution. The organics were dried over $MgSO_4$ and evaporated to give 4 (0.26 g, 81%). Recrystallization from toluene gave off-white needles. mp 193−195 °C (from toluene); ν_{max}(KBr disk)/cm^{-1} 1719 (w), 1649 (s), 1482 (w), 1423 (w), 1242 (m), 1075 (m), 1013 (m), 879, (m), 854 (s), 842 (s), 820 (s), 707 (w), 648 (w), 547 (w), 536 (w), 439 (m), 419 (m); ^{1}H NMR (500 MHz; $CDCl_3$) δ (ppm): 8.18 (2 H, s); ^{13}C NMR (125 MHz; $CDCl_3$) δ (ppm): 188.1, 152.8, 136.7, 114.9; *m*/*z* (EI) 225.9328 (calcd for $C_7H_2N_2OS_3$, 225.9329).

*6,6′-Bi-([1,3]dithiolo-[4,5-f][2,1,3]benzothiadiazolylidene) (**4**, BT-TTF).* A mixture of **3** (0.26g, 1.07 mmol) and degassed triethylphosphite (5 mL) was heated for 2 h at 120 °C. The reaction was cooled to room temperature and diluted with methanol before collecting the red solid via filtration. The insoluble solid (0.19 g, 85%) was washed with methanol, acetone, and dichloromethane before drying overnight under vacuum. Insoluble in common organic solvents, compound **4** was recrystallized from 1,2-dichlorobenzene to form red needles. Mp 464 °C (DSC from 1,2-dichlorobenzene); elemental anal. Found: C, 39.90; H, 0.87; N, 13.02. $C_{14}H_4N_4S_6$ requires C, 39.98; H, 0.96; N, 13.32%); ν_{max}(KBr disk)/cm^{-1} 1483 (w), 1430 (s), 1239 (s), 1072 (s), 852 (s), 818 (s), 778 (s), 699 (w), 670 (w), 642 (s), 529 (m), 405 (m); ^{1}H and ^{13}C NMR could not be determined due to poor solubility; *m*/*z* (EI) 419.8744 (calcd for $C_{14}H_4N_4S_6$, 419.8760).

2. 2. Characterization Methods. Differential scanning calorimetry (DSC) measurements were obtained on a TA Instruments Q20 at a heating rate of 10 °C/min under nitrogen. Thermal gravimetric analysis (TGA) was performed on a TA Instruments 2950 at a heating rate of 10 °C/min under nitrogen. A Perkin-Elmer Lamda 9 UV−vis-NIR spectrophotometer was used to measure optical absorption. Cyclic voltammetry (CV) was conducted in an electrolyte solution of 0.1 M tetrabutylammonium hexafluorophosphate in acetonitrile (thin film) or 1,2-dichlorobenzene (solution). A typical three-electrode cell was used with a working electrode (ITO glass for thin films and platinum for solution), a reference electrode (Ag/Ag^+, referenced against ferrocene/ferrocenium ($FeCp_2^{+/0}$)), and a counter electrode (Pt gauze) under a nitrogen atmosphere at a sweeping rate of 100 mV/s (CV-50W voltammetric analyzer, BAS). The onset potentials were determined from the intersection of two tangents drawn at the rising current and background current of the cyclic voltammogram. According to the redox onset potentials of the CV measurements, the HOMO/LUMO energy levels of the materials were estimated based on the reference energy level of ferrocene (4.8 eV below vacuum): HOMO/LUMO = $-(E_{onset} - 0.12\ V) - 4.8$ eV, where the value 0.12 V is for $FeCp_2^{+/0}$ vs Ag/Ag^+.[16]

2.3. BT-TTF Nanowire Synthesis. To a 50 mL round-bottom flask was added a mixture of 15 mL toluene and 5 mL chlorobenzene or other high boiling solvents (e.g., nitrobenzene or ODCB) and ∼0.02 g of BT-TTF powder. The solution was stirred with a magnetic device and the mixture brought to boiling until all the powder completely dissolved; the mixture was heated for an additional 5 min. Reduce the dimensions of the 1D crystals by adding 2−5 mL of methanol from a dropping funnel. Methanol was not added until the heat was completely turned off and the heating mantle device was removed from underneath the flask. ***Caution**: be certain to perform the*

dx.doi.org/10.1021/am3025036 | *ACS Appl. Mater. Interfaces* XXXX, XXX, XXX−XXX

experiment in a well-ventilated fume hood and utilize a Plexiglas guard shield for protection as addition of the methanol to the hot organic solvent can boil over and vigorously splash. Single-crystal nanowires immediately begin to form and within 30 min they can be collected from the organic solvent and transferred to methanol or ethanol for use in solvent-processed devices. Nanowire dimensions range from 100 to 200 μm in length and 1 to 2 μm in width. Addition of methanol (as mentioned above) reduces the widths (250 to 500 nm) with no significant change in nanowire lengths.

2.4. Device Fabrication (thin film). BT-TTF was deposited at 0.5 A/s from a resistively heated quartz crucible at 2×10^{-6} Torr, with the substrates at room temperature, 80, 100, and 120 °C. Interdigitated source (S) and drain (D) electrodes (W = 9000 μm, L = 90 μm, W/L = 100) were top-contact defined by evaporating a 50 nm thick gold film at 0.5A/s through a shadow mask (2×10^{-6} Torr). All OFET characterization was performed in air and completed within six hours of first exposure using an Agilent 4155B semiconductor parameter analyzer. The field-effect mobility was calculated in the saturation regime from the linear fit of $(I_{ds})^{1/2}$ versus V_{gs}. The threshold voltage (V_t) was estimated as the x intercept of the linear section of the plot of $(I_{ds})^{1/2}$ versus V_{gs}. The subthreshold swing was calculated by taking the inverse of the slope of I_{ds} versus V_{gs} in the region of exponential current increase.

2.5. Atomic Force Microscopy and Transmission Electron Microscopy. Digital Instruments Multimode Nanoscope IIIa scanning probe microscope was used in AFM taping mode. Tips were etched silicon tips with a typical resonant frequency of 300 - 350 kHz. BT-TTF single-crystal nanowires were examined using a Phillips EM420 electron microscope at an accelerating voltage of 100 kV. The samples for electron microscopy were prepared by drop-casting nanowires from a methanol dispersion onto a carbon-coated copper grid.

3. RESULTS AND DISCUSSION

3.1. Synthesis and Characterization of BT-TTF Molecule. BT-TTF was synthesized by phosphite-mediated self-coupling of [1,2,5]thiadiazolo[3,4-f][1,3]benzodithiole-2-one **3** (Scheme 1). Precursor **3** was prepared starting from the reductive cleavage of the thiocyanate substituents on 2,1,3-benzenethiadiazole-5,6-bis(thiocyanate) **1**[15a] in aqueous sulfide. In situ condensation with carbon disulfide afforded [1,2,5]-thiadiazolo[3,4-f][1,3]benzodithiole-2-thione **2** in 75% yield. Phosphite-mediated self-coupling of **2** resulted in poor yields (~10%) of the target compound, BT-TTF, and for that reason it was necessary to convert thione **2** into the corresponding ketone **3** with mercuric acetate. Treatment of **3** with triethylphosphite[15b,c] afforded BT-TTF, as a red solid, in 85% yield.

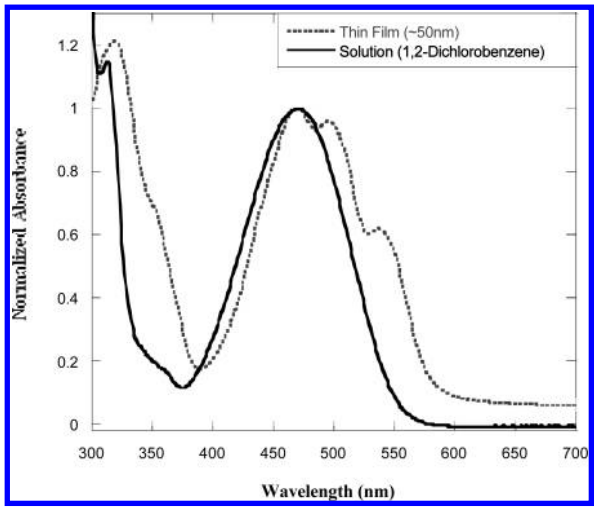

Figure 2. Normalized UV−vis absorption of BT-TTF as a thin film and in hot 1,2-dichlorobenzene.

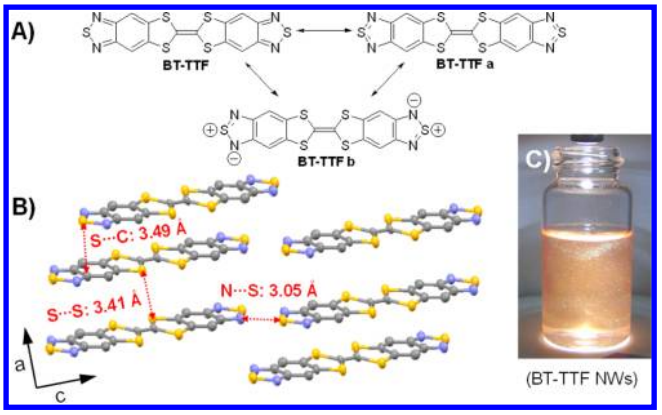

Figure 3. (A) Molecular structure and possible resonance contributors of BT-TTF; (B) molecular packing of BT-TTF illustrating π-stacking and intermolecular contacts; (C) an optical photograph of solvent-dispersed BT-TTF NWs (in MeOH).

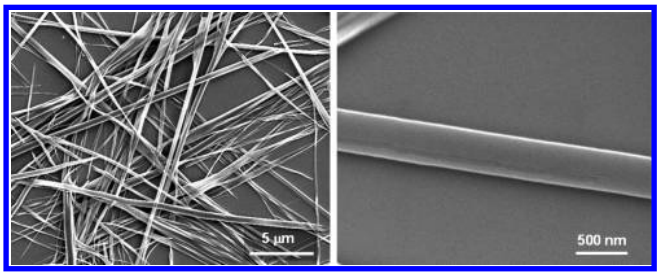

Figure 4. SEM images of BT-TTF single-crystal nanowires prepared by addition of methanol to recrystallization solvent.

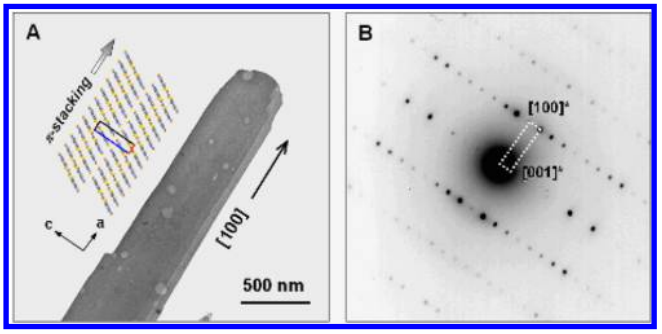

Figure 5. (A) TEM image of an individual BT-TTF single-crystal nanowire with the indicated crystallographic axis, i.e., [100]. The inset shows the molecular packing of BT-TTF molecules and the π-stacking along the a-axis; (B) Corresponding electron diffraction pattern. The diffraction spots were recorded in the [010] orientation, suggesting that the growth direction of the wire is along the [100] (i.e., the short unit cell axis a). The molecules exhibit a short stacking distance (3.487 Å).

Strong intermolecular interactions limit the solubility of BT-TTF compound in common organic solvents, though bulk quantities of nanowires could be prepared from hot 1,2-dichlorobenzene. Purification was carried out via sublimation and characterization was performed in both the solid state and in hot 1,2-dichlorobenzene. Thermal gravimetric analysis (TGA) showed an onset weight loss of 345 °C, however, there are no apparent transitions in the sealed-pan differential

dx.doi.org/10.1021/am3025036 | ACS Appl. Mater. Interfaces XXXX, XXX, XXX−XXX

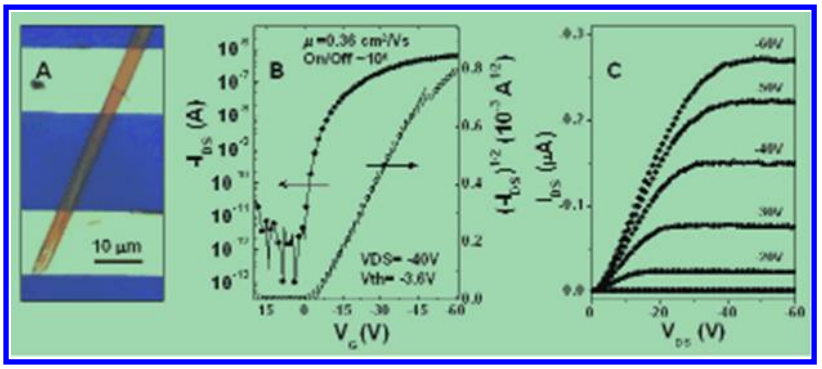

Figure 6. (A) Optical micrograph of individual BT-TTF single-crystal transistors; (B) transfer, and (C) output characteristicis. The output and transfer curves correspond to the optical micrograph shown in A.

Table 1. OTFT Data (average of six individual devices) of BT-TTF Fabricated at Various Substrate Deposition Temperatures[a]

T (°C)	μ_{sat} (cm^2/V s)	V_t (V)	S (V/dec)	I_{on}/I_{off}
25	2.01×10^{-4}	−10	2.0	1×10^3
80	1.91×10^{-3}	−8	1.6	1×10^5
100	4.57×10^{-4}	−11	1.8	1×10^4
120	4.68×10^{-4}	−12	1.8	1×10^4

[a]Channel width, W = 9000 μm; channel length, L = 90 μm; W/L = 100. μ_{sat}, saturation field-effect mobility; V_t, threshold voltage; S, subthreshold slope; and I_{on}/I_{off}, on/off current ratio.

scanning calorimetry (DSC) curve until a melting point/decomposition at 464 °C (Figure 1). We attribute the TGA anomaly to sublimation as traces of the molecules can be found on the upper portion of the furnace. Further evidence that BT-TTF is subliming rather than decomposing is found in the relative ease of crystal growth by physical vapor transport sublimation at 340 °C with no obvious color change of the sample. These high-temperature transitions demonstrate the good thermal stability of this material.

UV−visible spectroscopy and cyclic voltammetry (CV) were performed in hot 1,2-dichlorobenzene solutions and on thin films (Figure 2 and Figure S1 in the Supporting Information). The reason that thin film absorption spectrum exhibits two additional maxima is due to increased intermolecular interactions. The intermolecular interactions give rise to low-energy bands at 512 and 550 nm. Despite the electron withdrawing BT-moiety, no reduction was observed in either the thin film or solution CV. BT-TTF shows an irreversible oxidation as a thin film and an onset oxidation potential of 0.75 V ($FeCp_2^{+/0}$). From this we estimated a solid state HOMO energy level of −5.5 eV.[16] We estimated a LUMO energy level of −3.4 eV, using an optical band gap of 2.1 eV obtained from the thin film UV−vis absorption onset.

3.2. Bulk and Nanowire Single Crystals of BT-TTF Molecule. Single crystals of BT-TTF, obtained by physical vapor transport growth[7,8] were examined using X-ray crystallography to unambiguously determine the structure. Crystals belong to the triclinic space group P-1 (No.2) with a = 3.9206(4) Å, b = 6.9220(8) Å, c = 14.4072(16) Å, α = 77.661°(5), β = 83.708°(5), γ = 78.028°(6). As expected, BT-TTF is planar within the limits of error. S═N bond lengths (1.62 and 1.63 Å) are between that of S−N single bond[13a] (1.73 Å) and S═N double bond[13a] lengths (1.53 Å), whereas C═N double bonds are similar to those found in heterocycles.[17a] Although we can depict the intermediacy of all bond lengths (C═C double bond lengths range from 1.36 to 1.45 Å) with three resonance contributors, BT-TTF, BT-TTFa, and BT-TTFb (Figure 3A), the molecule shows alternations between single and double bond character, suggesting a dominance of the resonance form BT-TTF. The packing diagram of BT-TTF is shown in Figure 3B. BT-TTF forms 1D π-stacks with multiple interactions between neighboring sulfur, nitrogen, and carbon atoms. We observed short intermolecular S...S distances of 3.41 Å, S···C distances of 3.49 Å, and S···N contact distances of 3.05 Å. These values are shorter than the sum of the van der Waals radii.[17b] The thiadiazole moiety plays a key role in the solid state structure of the molecule and contributes to the high degree of order. A previous comparison of known literature values[8a] had shown an inverse correlation between the bond length and contact distance. Our data support these observations that attribute short thiadiazole contacts with electrostatic dipolar interactions between neighboring -NSN- linkages, as represented by BT-TTFb.

Scanning electron microscopy (SEM) images of BT-TTF single-crystal nanowires prepared by addition of methanol to recrystallization solvent are shown in Figure 4. Solvent-borne crystals dispersed in methanol (Figure 3C) were drop-cast onto copper grids and analyzed via transmission electron microscopy (TEM) and electron diffraction to determine the molecular packing of BT-TTF in 1D crystals. Figure 5A shows a TEM image of a BT-TTF nanowire and Figure 5B shows the corresponding electron diffraction. By indexing the reciprocal electron diffraction spots, we verified the real space packing of BT-TTF molecules within the nanowire. Molecules stack face-to-face along the [100] direction with intermolecular distances of 3.49 Å.

3.3. Nanowire and Thin-Film Transistors of BT-TTF Molecule. Single-crystal nanowire transistors were fabricated by drop-casting dispersions of BT-TTF nanowires from methanol directly onto bottom-contact gold source-drain electrodes. Gold electrodes and SiO_2 (300 nm) were modified with nitrobenzenethiol and OTS, respectively, in order to improve charge-injection and device characteristics.[18] Figure 6A shows a BT-TTF single-crystal transistor, whereas panels B and C show the electrical characteristics. A hole mobility, threshold voltage, and current on/off ratio of 0.36 $cm^2/(V\ s)$, −3.6 V, and ~1×10^6 were measured, respectively. Individual nanowire transistors showed average mobilities of 0.22 $cm^2/(V\ s)$ based on 20 measured devices. As a comparison, we also fabricated thin film transistors via thermal evaporation in a top-contact configuration and found the mobility to be dependent on the

dx.doi.org/10.1021/am3025036 | ACS Appl. Mater. Interfaces XXXX, XXX, XXX−XXX

substrate deposition temperatures. Mobilities in the range of 0.0002 to 0.002 $cm^2/(V\ s)$ were measured with the highest mobility observed at a substrate deposition temperature of 80 °C (Table 1). Thermal evaporation yields a network of poorly connected crystals (see Figure S2 in the Supporting Information) which significantly limits the mobility compared to single-crystal nanowires underscoring the applicability of solvent-dispersed crystals for high-performance transistor devices.

4. CONCLUSIONS

We have synthesized a new robust organic semiconductor, BT-TTF, and determined the structure, molecular packing and charge-transporting properties. Short intermolecular S···S, S···N, and S···C contacts define the solid state structure of BT-TTF single crystals which π-stack along the [100]. Solvent-cast single-crystal nanowire transistors showed mobilities as large as 0.36 $cm^2/(V\ s)$ with excellent device characteristics. This study further illustrates the impact of molecular design and a demonstration of high-performance single-crystal nanowire transistors from the resulting semiconductor.

■ ASSOCIATED CONTENT

Supporting Information

Thin film and solution CVs of BT-TTF, tapping mode AFM height images of BT-TTF on OTS/SiO_2 evaporated at different temperatures, X-ray data in CIF format. This material is available free of charge via the Internet at http://pubs.acs.org.

■ AUTHOR INFORMATION

Corresponding Author

*E-mail: ajen@u.washington.edu (A.K.-Y.J.); jenekhe@u.washington.edu (S.A.J.).

Notes

The authors declare no competing financial interest.

■ ACKNOWLEDGMENTS

This work is supported by AFOSR and the National Science Foundation (NSF-STC Program under Agreement DMR-0120967). A.K.-Y.J. acknowledges the Boeing-Johnson Professorship for its support.

■ REFERENCES

(1) (a) Murphy, A. R.; Fréchet, J. M. J. *Chem. Rev.* **2007**, *107*, 1066−1096. (b) Anthony, J. E. *Angew. Chem., Int. Ed.* **2008**, *47*, 452−483. (c) Allard, S.; Forster, M.; Souharce, B.; Thiem, H.; Scherf, U. *Angew. Chem., Int. Ed.* **2008**, *47*, 4070−4098.

(2) (a) Arias, A. C.; MacKenzie, J. D.; McCulloch, I.; Rivnay, J.; Salleo, A. *Chem. Rev.* **2010**, *110*, 3−24. (b) Anthony, J. E.; Facchetti, A.; Heeney, M.; Marder, S. R.; Zhan, X. W. *Adv. Mater.* **2010**, *22*, 3876−3892.

(3) (a) Takimiya, K.; Shinamura, S.; Osaka, I.; Miyazaki, E. *Adv. Mater.* **2011**, *23*, 4347−4370. (b) Wang, C. L.; Dong, H. L.; Hu, W. P.; Liu, Y. Q.; Zhu, D. B. *Chem. Rev.* **2012**, *112*, 2208−2267.

(4) (a) Forrest, S. R. *Nature* **2004**, *428*, 911−918. (b) Katz, H. E. *Chem. Mater.* **2004**, *16*, 4748−4756.

(5) (a) Zhang, L.; Di, C. A.; Yu, G.; Liu, Y. Q. *J. Mater. Chem.* **2010**, *20*, 7059−7073. (b) Sokolov, A. N.; Tee, B. C. K.; Bettinger, C. J.; Tok, J. B. H.; Bao, Z. N. *Acc. Chem. Res.* **2012**, *45*, 361−371.

(6) (a) Gelinck, G.; Heremans, P.; Nomoto, K.; Anthopoulos, T. D. *Adv. Mater.* **2010**, *22*, 3778−3798. (b) Sekitani, T.; Someya, T. *Adv. Mater.* **2010**, *22*, 2228−2246. (c) Tobjörk, D.; Österbacka, R. *Adv. Mater.* **2011**, *23*, 1935−1961.

(7) (a) Briseno, A. L.; Mannsfeld, S. C. B.; Ling, M.-M.; Liu, S.; Tseng, R. J.; Reese, C.; Roberts, M. E.; Yang, Y.; Wudl, F.; Bao, Z. N. *Nature* **2006**, *444*, 913−917. (b) Sundar, V. C.; Zaumseil, J.; Podzorov, V.; Menard, E.; Willett, R. L.; Someya, T.; Gershenson, M. E.; Rogers, J. A. *Science* **2004**, *303*, 1644−1646.

(8) (a) de Boer, R. W. I.; Gershenson, M. E.; Morpurgo, A. F.; Podzorov, V. *Phys. Status Solidi (a)* **2004**, *201*, 1302−1331. (b) Gershenson, M. E.; Podzorov, V.; Morpurgo, A. F. *Rev. Mod. Phys.* **2006**, *78*, 973−989.

(9) (a) Briseno, A. L.; Mannsfeld, S. C. B.; Jenekhe, S. A.; Bao, Z.; Xia, Y. *Mater. Today* **2008**, *11*, 38−47. and references therein (b) Briseno, A. L.; Mannsfeld, S. C. B.; Lu, X.; Xiong, Y.; Jenekhe, S. A.; Bao, Z.; Xia, Y. *Nano Lett.* **2007**, *7*, 668−675. (c) Briseno, A. L.; Mannsfeld, S. C. B.; Reese, C.; Hancock, J. M.; Xiong, Y.; Jenekhe, J. A.; Bao, Z.; Xia, Y. *Nano Lett.* **2007**, *7*, 2847−2853.

(10) (a) Kim, D. H.; Lee, D. Y.; Lee, H. S.; Lee, W. H.; Kim, Y. H.; Han, J. I.; Cho, K. *Adv. Mater.* **2007**, *19*, 678−682. (b) Li, R. J.; Hu, W. P.; Liu, Y. Q.; Zhu, D. B. *Acc. Chem. Res.* **2010**, *43*, 529−540. and references therein (c) Tang, Q. X.; Jiang, L.; Tong, Y. H.; Li, H. X.; Liu, Y. L.; Wang, Z. H.; Hu, W. P.; Liu, Y. Q.; Zhu, D. B. *Adv. Mater.* **2008**, *20*, 2947−2951 and references therein.

(11) (a) Moon, H.; Zeis, R.; Borkent, E.-J.; Besnard, C.; Lovinger, A. J.; Siegrist, T.; Kloc, C.; Bao, Z. N. *J. Am. Chem. Soc.* **2004**, *126*, 15322−15323. (b) Curtis, M. D.; Cao, J.; Kampf, J. W. *J. Am. Chem. Soc.* **2004**, *126*, 4318−4328. (c) Kim, F. S.; Ren, G. Q.; Jenekhe, S. A. *Chem. Mater.* **2011**, *23* (3), 682−732 and references therein.

(12) (a) Naraso, Nishida, J.; Kumaki, D.; Tokito, S.; Yamashita, Y. *J. Am. Chem. Soc.* **2006**, *128*, 9598−9599. (b) Mas-Torrent, M.; Durkut, M.; Hadley, P.; Ribas, X.; Rovira, C. *J. Am. Chem. Soc.* **2004**, *126*, 984−985. (c) Bendikov, M.; Wudl, F.; Perepichka, D. F. *Chem. Rev.* **2004**, *104*, 4891−4945.

(13) (a) Gieren, A.; Lamm, V.; Haddon, R. C.; Kaplan, M. L. *J. Am. Chem. Soc.* **1979**, *101*, 7277−7281. (b) Tomura, M.; Tanaka, S.; Yamashita, Y. *Heterocycles* **1993**, *35*, 69−72. (c) Ono, K.; Tanaka, S.; Yamashita, Y. *Angew. Chem., Int. Ed.* **1994**, *33*, 1977−1979.

(14) (a) Naraso, N. J.; Ando, S.; Yamaguchi, J.; Itaka, K.; Koinuma, H.; Tada, H.; Tokito, S.; Yamashita, Y. *J. Am. Chem. Soc.* **2005**, *127*, 10142−10143. (b) Okamoto, T.; Senatore, M. L.; Ling, M.-M.; Mallik, A. B.; Tang, M. L.; Bao, Z. N. *Adv. Mater.* **2007**, *19*, 3381−3384.

(15) (a) Brusso, J. L.; Clements, O. P.; Haddon, R. C.; Itkis, M. E.; Leitch, A. A.; Oakley, R. T.; Reed, R. W.; Richardson, J. F. *J. Am. Chem. Soc.* **2004**, *126*, 8256. (b) Gao, X. K.; Wang, Y.; Yang, X. D.; Liu, Y. Q.; Qiu, W. F.; Wu, W. P.; Zhang, H. J.; Qi, T.; Liu, Y.; Lu, K.; Du, C. Y.; Shuai, Z. G.; Yu, G.; Zhu, D. B. *Adv. Mater.* **2007**, *19*, 3037−3042. (c) Jia, C. Y.; Liu, S. X.; Tanner, C.; Leiggener, C.; Neels, A.; Sanguinet, L.; Levillain, E.; Leutwyler, S.; Hauser, A.; Decurtins, S. *Chem.—Eur. J.* **2007**, *13*, 3804−3812.

(16) We used the relations IP = $-(E_{onset} - 0.12\ V) - 4.8$ eV; see: Liu, M. S.; Luo, J.; Jen, A. K.-Y. *Chem. Mater.* **2003**, *15*, 3496−3500.

(17) (a) Pauling, L. *The Nature of the Chemical Bond*, 3rd ed.; Cornell University Press: Ithaca, NY, 1960; pp 300−308. (b) p 260, Table 7−20.

(18) Gundlach, D. J.; Jia, L.; Jackson, T. N. *IEEE Electron Device Lett.* **2001**, *22*, 571−573.